High Optical Response in Forward Biased (In,Ga)N–GaN Multiquantum-Well Diodes Under Barrier Illumination

Jose Luis Pau, Ryan McClintock, Can Bayram, *Member, IEEE*, Kathryn Minder, Donald Silversmith, *Fellow, IEEE*, and Manijeh Razeghi, *Fellow, IEEE*

***Abstract*—The authors report on the current–voltage (I–V) characteristic under forward biases obtained in low leakage, small size p-(In,Ga)N–GaN-n multiquantum well diodes. Under barrier illumination, the devices present a high optical response with capabilities to detect optical powers in the pW range without further amplification. This response is attributed to the screening of the internal electric fields. Recombination times of a few seconds are found to be associated to this mechanism. Moreover, a step-like feature is found in the I–V characteristic before the diode turn-on voltage. Our model proposes tunneling current through the multiquantum-well structure as responsible of this feature. Fast modulation of the tunneling effect under barrier illumination is used to evaluate the detection of low photon fluxes.**

***Index Terms*—Photocurrent gain, single photon detection, ultraviolet detectors, III-nitride.**

I. Introduction

FROM the first investigations in III-nitride semiconductors, the high responsivities observed in GaN photoconductors and the associated gain mechanisms attracted the attention of many groups [1]–[3]. Other structures and photocurrent gain mechanisms have been also studied in order to satisfy the need of high sensitivity ultraviolet (UV) detectors for visible- and solar-blind applications. Examples of this research are: carrier multiplication in avalanche photodiodes [4], [5], minority carrier trapping in Schottky barrier photodiodes [6], and more recently, piezoelectric field engineering in multiple-quantum-well (MQW) detectors [7]. However, only avalanche multiplication has demonstrated high enough gain ($> 10^6$) to show single photon detection capabilities [8], [9].

A wide variety of (Al,Ga)N detector structures have been extensively studied for visible- and solar-blind applications. For detection in the visible and UV-A, (In,Ga)N–GaN MQW structures have demonstrated reliable performances and internal gain mechanisms as active regions of p-n and Schottky barrier photodiodes [7], [10], [11]. The polarization fields in InGaN–GaN multiple-quantum-well structures introduce additional variables in the carrier recombination dynamics. Charge separation and long recombination times are more likely in the sawtooth potentials created by the piezoelectric effect. High electric fields in the wells and barriers also modify the absorption spectra through the quantum confined Stark and Franz-Keldysh effects, respectively. Although material defects such as Indium nonuniformities across the well and threading dislocations complicate the analysis, clear features of the presence of strong electric fields have been observed in multiple studies [12]–[14].

In this work, we investigate an unexpected photocurrent component observed in p-(In,Ga)N–GaN-n MQW diodes under forward biases just before the turn-on voltage. Spectral characteristics, linearity, and time response are shown and discussed. These results are interpreted taking into account the absorption in high electric fields, potential distribution and carrier transport. Its application for single photon detection is also discussed.

II. Sample Growth and Device Fabrication

The p-InGaN–GaN MQW-n structures were grown on a lateral epitaxial overgrowth (LEO) GaN template by metal organic chemical vapor phase deposition. Details of the LEO technique can be found elsewhere [15]. The n-layer consisted of a 1-μm-thick GaN:Si layer. The undoped active layer comprised three InGaN–GaN (3 nm/7 nm) quantum wells, and was capped with a 550-nm-thick GaN:Mg layer. The In content in the wells was about 17%. A reference p-i-n sample was also grown for the study. It had an intrinsic region thickness equal to the total length of the active region (30 nm) in the p-MQW-n structure, and was used to compare electro-optical properties, as described in Section VI.

Activation of the p-type GaN was achieved by rapid thermal annealing (RTA) at 1000 °C for 30 s. From Hall effect measurements in reference samples, electron and hole concentrations were determined to be 3×10^{18} cm^{-3} and 4×10^{17} cm^{-3} in the n- and p-type layers, respectively.

After surface treatment with HCl:$H_2$0 (1:1), Ni–Au 30Å/30Å is deposited as semitransparent contact and is annealed to achieve ohmic contact to p-type material. Mesas were defined by ECR-RIE with $SiCl_2$ and Ar plasmas. Ti–Au (400Å/1200Å) is deposited as the thick contact metal for both n- and p-type GaN. Device sizes ranged from 0.005 to 0.07 mm^2.

Manuscript received August 6, 2007; revised November 1, 2007. The work of J. L. Pau was supported in part by the Fulbright Association-Spain and the Spanish Ministry of Education and Science J. L. Pau. The work of K. Minder was supported in part by Motorola.

J. L. Pau, R. McClintock, C. Bayram, K. Minder, and M. Razeghi are with the Center for Quantum Devices, Department of Electrical Engineering and Computer Science, Northwestern University, Evanston, IL 60208-3129 USA (e-mail: j-vizcaino@northwestern.edu; r-mcclintock@northwestern.edu;cbayram@northwestern.edu; kathryn@northwestern.edu; razeghi@eecs.northwestern.edu).

D. Silversmith is with the Air Force Office of Scientific Research, Arlington, VA 22203 USA (e-mail: donald.silversmith@afosr.af.mil).

Digital Object Identifier 10.1109/JQE.2007.914766

0018-9197/$25.00 © 2008 IEEE

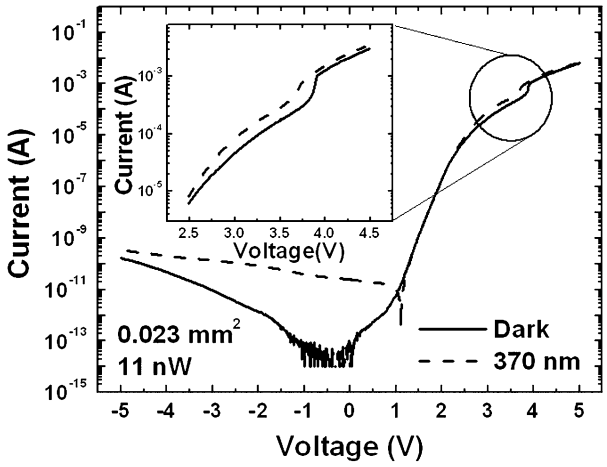

Fig. 1. Current–voltage characteristic measured in darkness (solid line) and under back-illumination (dashed line) with an optical power of 11 nW at 370 nm for a device area of 0.023 mm^2. Inset: Abnormal photocurrent signal under forward bias.

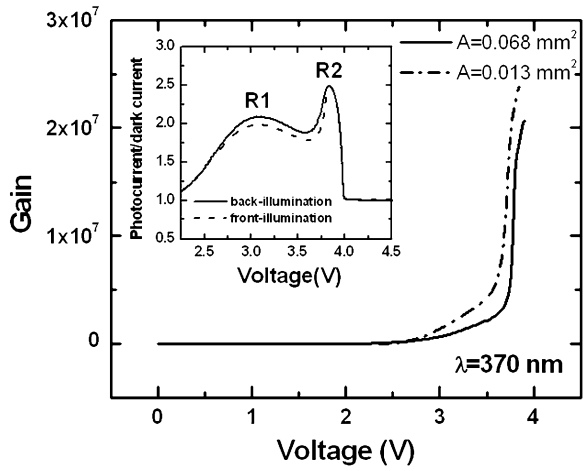

Fig. 2. Effective photocurrent gain obtained under illumination at 370 nm in devices with 0.068 (solid line) and 0.013 mm^2 (dashed line) areas. Inset: Photocurrent to dark current ratio under back- (solid line) and front-illumination (dashed line). The two bands obtained were labeled as R1 and R2.

III. Electrooptical Characteristics

Current–voltage (I–V) characteristics were measured in p-InGaN–GaN MQW-n diodes using an HP4155A Semiconductor Parameter Analyzer under back-illumination. A Xe lamp and a monochromator were used with a UV fiber-optic cable to couple the light, and allow back-illumination of the device. The input slit of the monochromator was adjusted to vary the photon flux, which was calibrated using a National Institute of Standards and Technology traceable UV-enhanced Si detector.

As shown in Fig. 1, devices presented two ranges of operation for light detection; one at reverse and low forward voltages, and other between 2.5 and 4.5 V forward bias. The photocurrent signal obtained in the first operation range is the result of the absorption in the active region, and increases slightly with reverse bias. This increase is attributed to a reduction of the carrier escape time from the well, which improves the external quantum efficiency [16].

The inset of Fig. 1 magnifies the second operation range in which an unexpected photocurrent signal is observed just before the turn-on voltage, as well as an unidentified step-like feature, near 4 V. This characteristic was observed in almost all of the diodes characterized, but they were most evident in the smallest area devices, i.e., those devices with less leakage current. Although the samples under study were grown on an LEO substrate to minimize leakage, we can rule out any effect of the LEO pattern, since the same behavior had been observed in devices on non-LEO substrates. In fact, a similar step-like feature has been observed before in InGaN–GaN Schottky photodiodes under high power excitation at similar voltages, as reported in [17].

From these measurements, an effective photoelectric gain value was calculated by using $G(V) = (I_{370\,\mathrm{nm}}(V) - I_{\mathrm{dark}}(V))/I_{370\,\mathrm{nm}}(0)$, where $I_{370\mathrm{nm}}$ and I_{dark} represent the current under 370 nm and no illumination, respectively, and V is the operation voltage. Fig. 2 shows the gain characteristic for two different size devices. Peak gain values in the 10^7 range were obtained; a high value obtainable in the past only by avalanche photodiodes. The gain was slightly higher for smaller area devices. The inset of Fig. 2 shows the photocurrent signal relative to the dark current, which reveals two prominent humps under back- or front-illumination with maximums at about 3 V (R1) and 3.8 V (R2), the latter corresponding to the onset voltage of the step-like feature. The origin of these two humps will be discussed later.

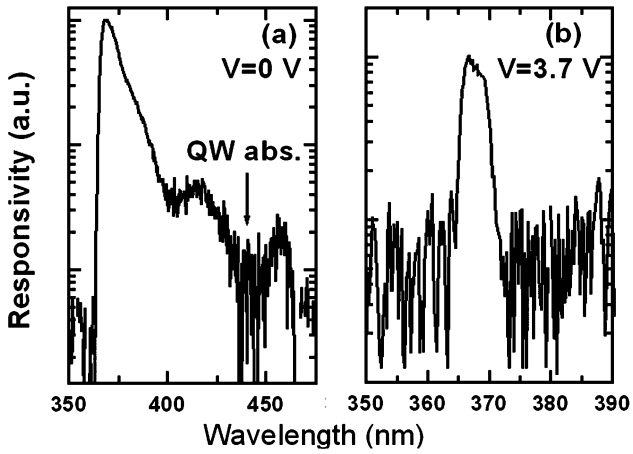

Fig. 3. Spectral response of the p-MQW-n diodes measured at (a) 0V and at (b) 3.7 V. The onset of the quantum well absorption is indicated. The incident optical power is less than 1 nW across the whole range.

The spectral response of the devices under back-illumination was measured at zero bias, in the absence of any gain mechanism, and at 3.7 V (Fig. 3). Under this illumination scheme, the GaN substrate helps to filter out the light with $\lambda < 363$ nm with a very high rejection ratio [18], making these detectors well suited to use in detection of intrinsic fluorescence of biological agents in combination with deep-UV light emitting diodes. At zero bias, the long wavelength response onset situates around 440 nm [Fig. 3(a)], in good agreement with the absorption onset in the quantum wells. However, under forward biases, the spectral characteristic of the response differs significantly, as shown in Fig. 3(b). The device is only sensitive to a very narrow band from 364 nm (GaN bandgap) to 372 nm.

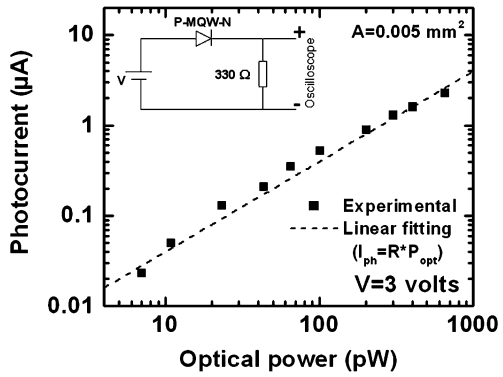

Fig. 4. Power-dependent measurements obtained from a 0.005 mm^2 area diode at 3 V. The dashed line is the linear fitting using $I_{\rm ph} = R \cdot P_{\rm opt}$, for which $I_{\rm ph}$ is the photocurrent defined as the total current minus the dark current, $P_{\rm opt}$ is the optical power, and R is the responsivity that acts as fitting parameter. Inset: Experimental setup.

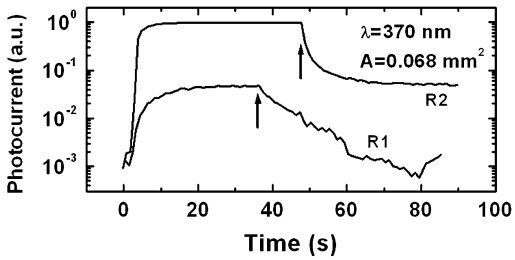

Fig. 5. Time response of a 0.068-mm^2 diode obtained during illumination at 370 nm at 3 V (R1) and 3.8 V (R2). The dark current level at t=0 s was subtracted for clarity. The arrows indicate the turn-off. The incident optical power was about 5 nW.

In order to study the linearity of this response, a 0.005 mm^2 device was biased at 3 V, i.e., the voltage that maximized the R1 band, in series with a 330 Ω load resistor (inset, Fig. 4). The current was measured via the voltage drop in the resistor using an oscilloscope. The device was illuminated with optical powers less than 1 nW. As observed in Fig. 4, photocurrent scales linearly with optical power, with a peak responsivity of about 4000 A/W. The minimum illumination detected without any further amplification or lock-in technique was 8 pW. The minimum detectable illumination increased slightly with device area; thus, 15 pW were needed to produce a significant change over the dark current level in 0.023 mm^2 devices.

The temporal response of the device at 3 V (R1) and at 3.8 V (R2) was measured (Fig. 5). The response at 3.8 V presented a faster rise time than at 3 V. However, whereas the sample biased at 3 V recovers its baseline dark current after illumination within tens of seconds, at 3.8 V, the current decreases following a nonexponential characteristic, eventually plateauing at an elevated current. The current difference between these two levels corresponds to the amplitude of the step-like feature observed in the I–V characteristic, and it can be attributed to an optically induced transition between two states of the device. This result evidences two different physical origins for the R1 and R2 gain bands.

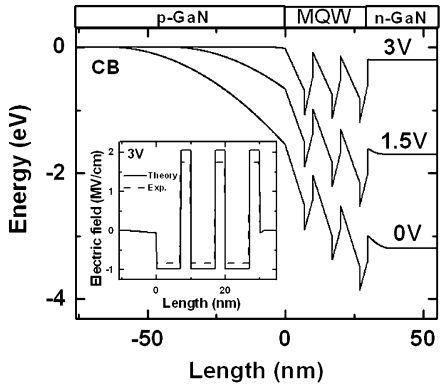

Fig. 6. Conduction band (CB) diagram at 0, 1.5, and 3 V calculated from (1). Inset: Electric fields calculated from the experimental and theoretical values for the piezoelectric constants given in [12] and [22], respectively.

IV. Band Diagram

In order to find out the origin of the spectral response characteristic under forward bias, we investigated the band structure. The resolution of the Poisson equation allows us to determine the potential distribution $(V(x))$ in the active region [19]. As a first approximation, we assumed that all the quantum wells are inside the depletion region, and that any unintentional doping there is much lower than the doping of the p-and n-type layers. The piezoelectric field in the growth direction (F_z) was calculated from $F_z = P_z/\varepsilon_s$, where P_z is the polarization as defined in [20], and ε_s is the dielectric permittivity of GaN. From the linear interpolation between GaN and InN, a 12% difference between the permittivities of GaN and $In_{0.17}Ga_{0.83}N$ is estimated. However, this has minimal effect compared to the polarization, and this difference is neglected in the analysis. Then, the analytical solution of the Poisson equation can be expressed as

$$V(x)=\begin{cases} 0, & x<-x_p \\ qN_a(x+x_p)^2/2\varepsilon_s, & -x_p<x<0 \\ \frac{qN_a}{\varepsilon_s}x_p x+\frac{qN_a}{2\varepsilon_s}x_p^2 & \\ +F_z(\frac{L_b}{L_w+L_b}x-l_w(x)), & 0<x<W \\ -\frac{qN_d}{2\varepsilon_s}[x-(W+x_n)]^2+V_0, & W<x<W+x_n \\ V_0, & x>W+x_n \end{cases} \tag{1}$$

where q is the electron charge, N_a is the acceptor concentration, N_d is the donor concentration, x_p and x_n are the boundaries of the space charge region in the p- and n-sides, respectively, L_b is the barrier length, L_w is the well width, W is the total length of the active region, l_w is the total length of the quantum wells for a distance lower than x, and $V_0 = V_{\rm bi} - V_a$, where $V_{\rm bi}$ is the built-in voltage and V_a is the applied voltage. The x_n and x_p distances can be calculated from

$$\begin{aligned} V_0 &= \frac{qN_a}{\varepsilon_s}x_p W+\frac{qN_a}{2\varepsilon_s}x_p^2+\frac{qN_d}{2\varepsilon_s}x_n^2 \\ N_a x_p &= N_d x_n \end{aligned} \tag{2}$$

taking into account charge neutrality. The potential calculated in this way allows us to obtain the band structure analytically, after adding the band-offsets at the InGaN-GaN interfaces [21]. The results for the conduction band diagram are shown in Fig. 6 at different forward biases.

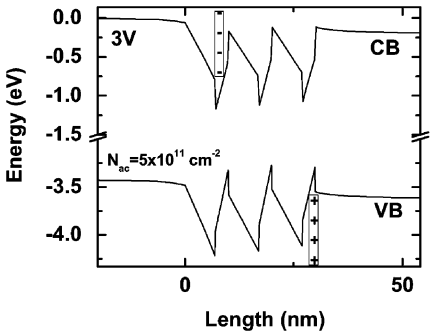

Fig. 7. Charge accumulation at the edges of the MQW region predicted by [25] under high injection conditions. The band diagram was calculated as the sum of (1) and the potential of the dipole when the accumulated charge is 5×10^{11} cm^{-2} in the first (electrons) and last (holes) wells.

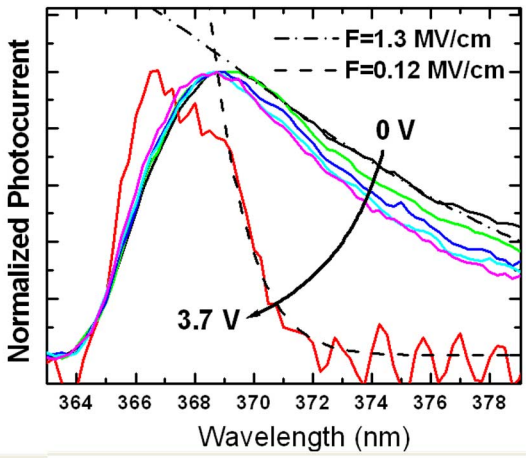

Fig. 8. Photocurrent measurements obtained in the p-MQW-n diodes at different forward biases ranging from 0 to 3.7 V (0, 0.25, 0.50, 0.75, 1, and 3.7 V). The dotted-dashed line represents the fitting to the photocurrent curve at 0 V using (3). The dashed line represents the fitting at 3.7 V. The electric field values obtained in each case are included.

From the derivative of the potential, we can obtain the electric field distribution. The experimental values of the polarization in InGaN–GaN QWs found in the literature are slightly lower than the theoretical ones; in the inset of Fig. 6, we compare the electric field strength provided by the experimental [12] and theoretical [22] piezoelectric constants, interpolating linearly to determine the InGaN constants in both cases. Using the theoretical values, electric field strengths of 1.4 MV/cm and 0.96 MV/cm are predicted in the barriers at 0 and 3.0 V, respectively. On the other hand, experimental values yielded electric fields of 1.2 MV/cm and 0.83 MV/cm at the same voltages. However, our analysis neglects the screening effect induced by the current flow and a self-consistent Poisson-Schrodinger calculation with time dependency would be needed to account for this. At 0 V, there is no screening effect induced by current injection, and the calculated electric field should be reliable. In fact, similar electric fields have been calculated in the literature [23]–[25]. Contrarily, the screening effects at forward bias voltages cannot be completely neglected. Actually, a situation of negative average electric field (NAE) has been predicted in [25] at forward biases just below the flat-band condition, leading to consequent electron and hole accumulation at the edges of the quantum well region. This charge distribution is depicted in Fig. 7, in which we have superimposed the potential created by a hypothetical dipole caused by the accumulation of electrons and holes in the first and last wells, respectively. We believe that this is likely to be the case in our devices at 3 V. The flat-band condition will be reached at slightly higher voltages, when the charge accumulated at the edges begins to re-distribute uniformly in the three wells: this process may occur by thermionic emission or tunneling. This redistribution gives rise to the step-like feature found in the *I–V* characteristics. The observation of a similar feature in InGaN–GaN MQW Schottky barrier photodiodes with NAE seems to support this hypothesis [7], [17].

V. Barrier Electric Field

From the previous discussion, it is expected that the strong electric fields in the barriers play an important role in the absorption close to the GaN band-edge [26].

Photocurrent (I_{ph}) measurements under back-illumination of the p-MQW-n diodes provided the spectra shown in Fig. 8 as a function of bias. The strong increase of the photocurrent from 378 to 370 nm suggests that the barrier absorption dominates the response in this spectral range. As the bias is increased, a shift and narrowing of the longer wavelength cut-off occurs in that region.

In order to estimate the total electric field strength (polarization and built-in), the data were fitted using the absorption coefficient dependence on the electric field, and taking into account that the $I_{\text{ph}} \propto \alpha$ approximation is reasonably valid when $\alpha L_i << 1$, L_i being the thickness of the intrinsic region. Therefore, in the Wentzel–Kramers–Brillouin approximation [27], the photocurrent can be fitted using

$$I_{\text{ph}}(h\nu) \propto \exp\left[-\frac{4\sqrt{2m_\mu}(E_{\text{gap}} - h\nu)^{3/2}}{3\,qF\hbar}\right] \qquad (3)$$

where E_{gap} is the energy gap, $h\nu$ is the photon energy, m_μ is the reduced effective mass, and F is the electric field. It is important to notice that this approximation is only valid for systems without quantum confinement, so it only accounts for the barrier absorption but not for the quantum well absorption. From (3), we can obtain the electric field strength in the barrier of the p-MQW-n diodes. Fig. 8 depicts the result of this fitting at 0 and 3.7 V. The average electric field, obtained after fitting three different diodes, is 1.3 $\pm$0.2 MV/cm at 0 V and 0.12 $\pm$0.05 MV/cm at 3.7 V. The first value is in fairly good agreement with the calculated values provided by (1). The blue-shift and narrowing of the cut-off also agrees with the decreasing value of the electric field in the barriers predicted by our analysis.

The electric field value at 3.7 V is significantly lower than the calculated value. The reason is that, as previously mentioned, our analysis cannot account for screening effects due to carrier injection under forward biases. Photocurrent provides an excellent way to get the electric field experimentally under those conditions. The quantum well absorption and subsequent photocurrent might lead us to overestimate the electric field slightly at low forward biases. However, its effect seems negligible at 3.7 V, at which point the cut-off becomes very sharp and no

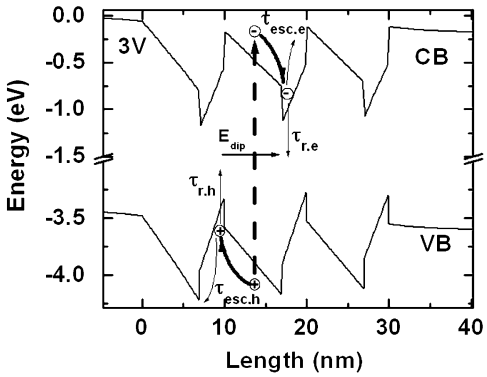

Fig. 9. Scheme of the electron–hole pair generation in the barriers and relaxation to the adjacent wells. $E_{\rm dip}$ represents the created dipole, and $\tau_{r,i}$ and $\tau_{{\rm esc},i}$ the recombination and escape times from the wells for electrons (e) and holes (h).

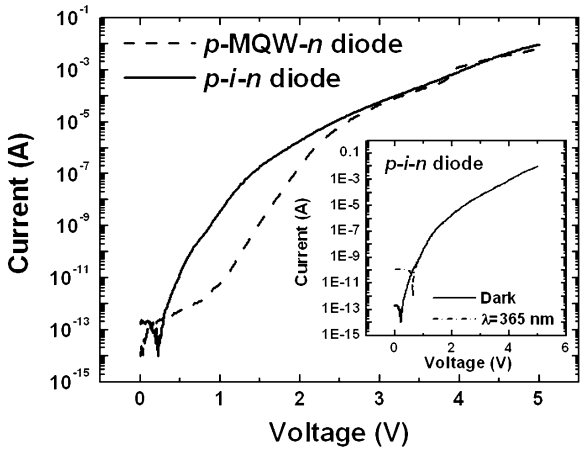

Fig. 10. I–V characteristics obtained in darkness from the p-MQW-n diodes under study and p-i-n diodes with an i-region thickness of 30 nm. Inset: I–V characteristics of the p-i-n diodes in darkness and under back-illumination at 365 nm.

response is observed above 372 nm. Therefore, this method enables the measurement of the electric fields in the barriers, which are crucial elements in the inter-well transport.

VI. Model and *I–V* Curve Analysis

From the charge accumulation depicted in Fig. 7, one can analyze the consequences of the barrier absorption. Carriers photogenerated in the barriers are going to be quickly separated and trapped in the adjacent wells. There, they form a dipole that screens the electric field in the barrier, enhancing the thermionic emission over the barrier and the tunneling probability, resulting in a total increase in the device current. The dipole field opposes the electric field of the long-range potential created by the accumulated charge at the edges of the MQW region, and makes the band diagram approach a flat-band situation: Fig. 9 illustrates this process. The escape $(\tau_{\rm esc})$ and recombination (τ_r) times of electrons and holes will determine the lifetime (τ) of this dipole.

Once the flat-band condition is reached, the charge distributes uniformly across the wells either by tunneling or by thermionic emission. The step-like feature is the result of this process, which is accompanied by a stronger luminescence observed from visual inspection through a microscope due to the enhanced recombination rate. This behavior was also observed at 77 K, which suggests a dominant tunneling process less sensitive to thermal effects, and accounts for the transition between device states (from NAE to flat-band diagram) found for the gain band R2 in the time response measurements. However, the characteristic time of this process remains uncertain from those measurements because it is masked by the long response times of the potential screening. This point will be elucidated in Section VII.

In order to gain further insight into the conduction mechanisms, the I–V characteristics of standard p-i-n diodes and p-MQW-n diodes were compared (Fig. 10). The thickness of the intrinsic region in the p-i-n diodes was equal to the total thickness of the active region in the p-MQW-n diodes. Two main differences are noticeable between both I–V characteristics. One is the right-shift of the p-MQW-n curve at low voltages; this shift is caused by the extra potential drop $(\phi_{\rm MQW})$ in the heterojunctions forming the MQW region, which is enhanced by the presence of piezoelectric fields [7]. The other difference is that the p-i-n diodes do not present the step-like feature, and in fact, no optical response was observed at that range of voltages (inset of Fig. 10). This confirms that both phenomena are a direct consequence of the MQW.

The general model for the I–V characteristic in p-i-n diodes is given by

$$I = I_0 \exp[qV/\eta kT] \,(\text{with } V > 3kT/q) \tag{4}$$

where I_0 is the saturation current, k is the Boltzmann constant, T is the temperature and η is the ideality factor. We neglect the effect of the series resistance for the sake of clarity. Using this equation, an $\eta = 3.7$ is obtained from the fitting of the p-i-n diodes at low voltages. This high ideality factor departs from the Sah–Noyce–Shockley theory, which is a typical characteristic of III-nitride diodes [28]. A possible explanation might be a slight Schottky rectifying behavior of the p-GaN contact.

From the I–V characteristics, the effect of the MQWs can be taken into account including an extra potential drop term $(\phi_{\rm MQW})$. Therefore

$$I = I_0 \exp[q(V - \phi_{\rm MQW})/\eta kT]. \tag{5}$$

The $\phi_{\rm MQW}$ obtained from the fitting of the p-MQW-n sample at low voltages is 0.62 V, while the ideality factor is equal to 3.7, as in the p-i-n diode. At high voltages, the potential drop at the heterojunctions is reduced by two effects: the screening of the piezoelectric field caused by the injection of carriers and, under illumination, the screening caused by photogenerated carriers in the barrier, as described previously. Then, two terms can be added to account for both effects

$$\phi_{\rm MQW} = \phi_0 - \phi_{\rm inj}(I) - \phi_{\rm ph}(P_{\rm opt}) \tag{6}$$

where $\phi_{\rm inj}$ and $\phi_{\rm ph}$ represent the lowering effect on the potential drop due to the current injection and optical power excitation $(P_{\rm opt})$, respectively. At low optical powers, we may consider as a first order approximation that $\phi_{\rm inj}(I_{\rm dark}) \approx \phi_{\rm inj}(I_{\rm il})$, which

allows us to calculate the ratio between the current under illumination ($I_{\rm il}$) and in darkness ($I_{\rm dark}$) as

$$\frac{I_{\rm il}}{I_{\rm dark}} = \exp[q\phi_{\rm ph}(P_{\rm opt})/\eta kT]. \tag{7}$$

The lowering effect on the barriers due to the optical power excitation can be written as

$$\phi_{\rm ph}(P_{\rm opt}) = \frac{P_{\rm opt}\tau(1-\exp(-\alpha N_b L_b))}{\varepsilon_s A} nL_b \tag{8}$$

where τ is the dipole lifetime, A the illuminated area, N_b is the number of barriers, α is the absorption coefficient and L_b the barrier length. Hence, from (7) and (8), we can determine approximately the dipole lifetime needed to get the $I_{\rm il}/I_{\rm dark}$ values measured in the samples under study. At 11 nW, this ratio was about 2 under uniform illumination across a 0.023 mm^2 area device. An absorption coefficient of 2.8×10^4 cm^{-1} is expected for the electric field calculated in the barriers. These values yield a dipole lifetime of 0.01 s. In our model, the dipole lifetime is given by $\tau^{-1} = 1/\tau_r + 1/\tau_{\rm esc}$. From the temporal response plot, τ_r can be estimated to be a few seconds. Therefore, our model predicts almost three orders of magnitude lower dipole lifetime, which means that the carrier escape time from the wells may dominate the dipole quenching.

At low powers, (7) can be approximated by

$$\frac{I_{\rm il}}{I_{\rm dark}} \approx 1 + q\phi_{\rm ph}(P_{\rm opt})/\eta kT \tag{9}$$

$$I_{\rm ph} = \frac{I_{\rm il} - I_{\rm dark}}{I_{\rm dark}} \approx q\phi_{\rm ph}(P_{\rm opt})/\eta kT \tag{10}$$

which accounts for the linear dependence of the photocurrent on incident power observed in our experiments for the gain band R1.

On the other hand, the R2 band is the result of the tunneling current that leads to the flat-band condition. The electrons and holes accumulated at the edges of the active region under high carrier injection travel through the barriers to meet in the wells. The barrier illumination screens part of the potential at the heterointerfaces, which is enhanced by the polarization fields, and increases the tunneling probability. Thus, the transition from NAE to the flat-band condition takes place at slightly lower voltages (see inset Fig. 1). The high current delivered makes this gain mechanism promising for high sensitivity detection.

VII. Detection of Low Photon Fluxes

We explore the use of the tunneling origin of band R2 to detect low photon fluxes. As concluded from the previous discussion, the illumination of the barriers helps to screen the potential at the heterointerfaces, enhancing tunneling probability and its associated current. Biasing the device at those voltages, we prepare it to trigger the tunneling process in presence of light. The device is kept biased for a short time, after which it is biased back to zero to sweep the charges from the wells. This operation mode is similar to the pulsed Geiger mode operation of avalanche photodiodes using a gated quenching circuit, but with a much lower baseline voltage.

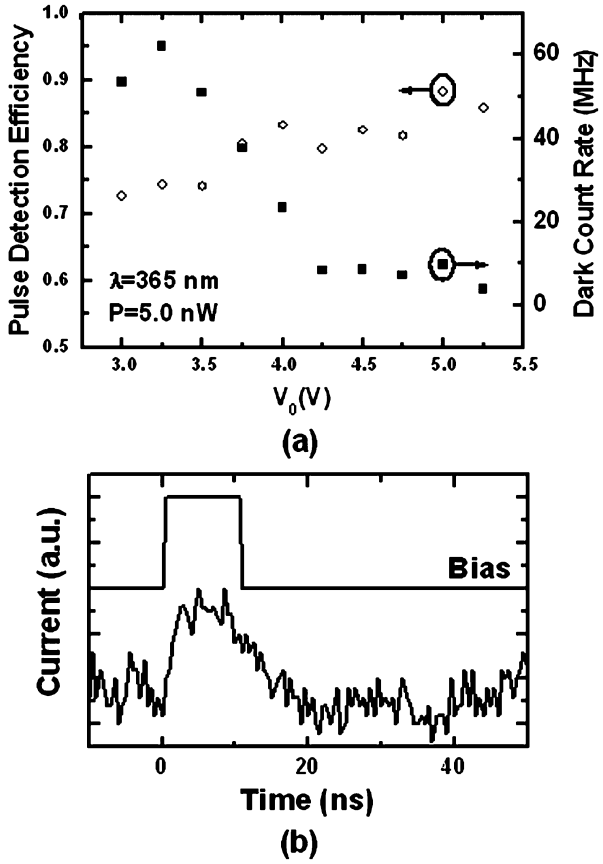

Fig. 11. (a) Left axis: Detection efficiency of 10 ns bias pulses with a V_0 amplitude under illumination with 5.0 nW ($\sim$ 90 ph/pulse). Right axis: Dark count rates. (b) Bias pulse applied to the device for detection of low photon fluxes, and current pulse delivered under barrier illumination; in the absence of illumination, the current remains below the noise floor.

To test this procedure, the device was biased using a pulse of amplitude $V_0 = 3 - 5.2$ V and width 10 ns at a repetition rate of 10 kz. The device was biased to zero in between pulses. The cathode of the device was connected to the 50-Ω input of a pulse counter [9]. The discriminator voltage of the pulse counter was adjusted to maximize the pulse detection efficiency and minimize the dark count rate. An optical power of 5 nW at 365 nm, equivalent to $\sim$ 90 ph/pulse, was used to pump the diode under back-illumination. The pulse detection probability was measured as the number of detected pulses divided by the total number of bias pulses. The dark count rate (DCR) is the probability of detecting a false count divided by our pulse width.

Fig. 11 (a) shows that DCR reduces from 54 MHz, at a pulse bias of 3 V, to 4 MHz at 5.25 V, whereas the pulse detection efficiency monotonously increases, reaching a value of 86% at 5.25 V. Most part of the DCR reduction takes place between 3.5 and 4.25 V, i.e., voltages that maximize R2 gain band. This reduction is due to the higher signal obtained when the amplitude of the bias pulse reaches this gain band. The tunneling process responsible of this mechanism delivers significant current pulses when the barriers are illuminated, as shown in Fig. 11(b). In contrast to the long-range potential screening, it demonstrates to be a fast process with characteristic times in the nanosecond range that enables the detection of low photon fluxes. Although, this

performance is still far from the current state-of-the-art of UV single-photon detectors based on APDs [29], [9], investigation of these devices is worthwhile since it may lead to revolutionary advantages such as lower bias voltages, larger active areas, or uniform response in the single-photon detection field.

VIII. Conclusion

High optical responses have been obtained under barrier illumination in forward biased p-InGaN–GaN MQW-n diodes. Photocurrent measurements allowed us to evaluate the effect of the polarization fields on the barrier absorption, in good agreement with theoretical predictions. Two gain mechanisms are identified: the long-range inter-well potential screening (R1) and the tunneling effect through the barriers (R2). The first gain mechanism has demonstrated to be slow, with response times of seconds. On the other hand, the tunneling effect has demonstrated to enable the fast detection of low photon fluxes. A coupled Schrodinger–Poisson solver might help to confirm the resonant origin of the tunneling mechanism.

References

[1] M. A. Khan, J. N. Kuznia, D. T. Olson, J. M. V. Hove, M. Blasingame, and L. F. Reitz, "High-responsivity photoconductive ultraviolet sensors based on insulating single-crystal GaN epilayers," *Appl. Phys. Lett.*, vol. 60, pp. 2917–2919, Jun. 1992.

[2] E. Muñoz, E. Monroy, J. A. Garrido, I. Izpura, F. J. Sanchez, M. A. Sanchez-Garcia, E. Calleja, B. Beaumont, and P. Gibart, "Photoconductor gain mechanisms in GaN ultraviolet detectors," *Appl. Phys. Lett.*, vol. 71, pp. 870–872, Aug. 1997.

[3] F. Binet, J. Y. Duboz, E. Rosencher, F. Scholz, and V. Harle, "Mechanisms of recombination in GaN photodetectors," *Appl. Phys. Lett.*, vol. 69, pp. 1202–1204, Aug. 1996.

[4] R. McClintock, J. L. Pau, K. Minder, C. Bayram, P. Kung, and M. Razeghi, "Hole-initiated multiplication in back-illuminated GaN avalanche photodiodes," *Appl. Phys. Lett.*, vol. 90, p. 141112, Apr. 2007.

[5] J. B. Limb, D. Yoo, J. H. Ryou, W. Lee, S. C. Shen, R. D. Dupuis, M. L. Reed, C. J. Collins, M. Wraback, D. Hanser, E. Preble, N. M. Williams, and K. Evans, "GaN ultraviolet avalanche photodiodes with optical gain greater than 1000 grown on GaN substrates by metal-organic chemical vapor deposition," *Appl. Phys. Lett.*, vol. 89, p. 011112, Jul. 2006.

[6] O. Katz, V. Garber, B. Meyler, G. Bahir, and J. Salzman, "Gain mechanism in GaN Schottky ultraviolet detectors," *Appl. Phys. Lett.*, vol. 79, pp. 1417–1419, Sep. 2001.

[7] C. Rivera, J. L. Pau, and E. Muñoz, "Photocurrent gain mechanism in Schottky barrier photodiodes with negative average electric field," *Appl. Phys. Lett.*, vol. 89, p. 263505, Dec. 2006.

[8] S. Verghese, K. A. McIntosh, R. J. Molnar, L. J. Mahoney, R. L. Aggarwal, M. W. Geis, K. M. Molvar, E. K. Duerr, and I. Melngailis, "GaN avalanche photodiodes operating in linear-gain mode and Geiger mode," *IEEE Trans. Electron Devices*, vol. 48, no. 3, pp. 502–511, Mar. 2001.

[9] J. L. Pau, R. McClintock, K. Minder, C. Bayram, P. Kung, M. Razeghi, E. Muñoz, and D. Silversmith, "Geiger-mode operation of back-illuminated GaN avalanche photodiodes," *Appl. Phys. Lett.*, vol. 91, p. 041104, Jul. 2007.

[10] J. L. Pau, J. Anduaga, C. Rivera, A. Navarro, I. Alava, M. Redondo, and E. Muñoz, "Optical sensors based on III-nitride photodetectors for flame sensing and combustion monitoring," *Appl. Opt.*, vol. 45, pp. 7498–7503, Oct. 2006.

[11] Y.-Z. Chiou, Y.-K. Su, S.-J. Chang, J. Gong, Y.-C. Lin, S.-H. Liu, and C.-S. Chang, "High detectivity InGaN-GaN mutiquantum well $p-n$ junction diodes," *IEEE J. Quantum Electron.*, vol. 39, no. 5, pp. 681–685, May 2003.

[12] A. Hangleiter, F. Hitzel, S. Lahmann, and U. Rossow, "Composition dependence of polarization fields in GaInN–GaN quantum wells," *Appl. Phys. Lett.*, vol. 83, pp. 1169–1171, Aug. 2003.

[13] A. N. Cartwright, P. M. Sweeney, T. Prunty, D. P. Bour, and M. Kneissl, "Electric field distribution in strained p-i-n GaN–InGaN multiple quantum well structures," *MRS Internet J. Nitride Semicond. Res.*, vol. 4, no. 12, 1999.

[14] H. Kollmer, J. S. Im, S. Heppel, J. Off, F. Scholz, and A. Hangleiter, "Intra- and interwell transitions in GaInN–GaN multiple quantum wells with built-in piezoelectric fields," *Appl. Phys. Lett.*, vol. 74, pp. 82–84, Jan. 1999.

[15] M. Razeghi, P. Kung, D. Walker, M. Hamilton, and J. Diaz, "High quality LEO growth and characterization of GaN films on Al_2O_3 and Si substrates," *Proc. SPIE*, vol. 3725, pp. 14–20, Apr. 1999.

[16] C. Rivera, J. L. Pau, A. Navarro, and E. Muñoz, "Photoresponse of (In,Ga)N-GaN multiple-quantum-well structures in the visible and UVA ranges," *IEEE J. Quantum Electron.*, vol. 42, no. 1, pp. 51–58, Jan. 2006.

[17] C. Rivera, J. L. Pau, J. Pereiro, and E. Muñoz, "Properties of Schottky barrier photodiodes based on InGaN–GaN MQW structures," *Superlattices Microstruct.*, vol. 36, pp. 849–857, Oct.–Dec. 2004.

[18] J. L. Pau, C. Rivera, J. Pereiro, E. Muñoz, E. Calleja, U. Schühle, E. Frayssinet, B. Beaumont, J. P. Faurie, and P. Gibart, "Nitride-based photodetectors: From visible to x-ray monitoring," *Superlattices Microstruct*, vol. 36, pp. 807–814, Oct.–Dec 2004.

[19] S. M. Sze and K. K. Ng, *Physics of Semiconductor Devices*. Hoboken, NJ: Wiley, 2007, ch. 2.

[20] A. Bykhovski, B. Gelmont, and M. Shur, "The influence of the strain-induced electric field on the charge distribution in GaN-AlN-GaN structure," *J. Appl. Phys.*, vol. 74, pp. 6734–6739, Dec. 1993.

[21] H. Zhang, E. J. Miller, E. T. Yu, C. Poblenz, and J. S. Speck, "Measurement of polarization charge and conduction-band offset at $In_xGa_{1-x}N$–GaN heterojunction interfaces," *Appl. Phys. Lett.*, vol. 84, pp. 4644–4646, Jun. 2004.

[22] F. Bernardini, V. Fiorentini, and D. Vanderbilt, "Spontaneous polarization and piezoelectric constants of III-V nitrides," *Phys. Rev. B*, vol. 56, pp. R10 024–R10 027, Oct. 1997.

[23] U. M. E. Christmas, A. D. Andreev, and D. A. Faux, "Calculation of electric field and optical transitions in InGaN–GaN quantum wells," *J. Appl. Phys.*, vol. 98, p. 073522, Oct. 2005.

[24] D. Oriato and A. B. Walker, "Effects of piezoelectric field, bias and indium fluctuations on a InGaN-GaN single quantum well system," *Physica B*, vol. 314, pp. 59–62, Mar. 2002.

[25] H. Wenzel, "Accurate modeling of InGaN quantum wells," *Opt. Quantum Electron.*, vol. 38, no. 9, pp. 953–961, Sep. 2006.

[26] F. Binet, J. Y. Duboz, E. Rosencher, F. Scholz, and V. Härle, "Electric field effects on excitons in gallium nitride," *Phys. Rev. B*, vol. 54, pp. 8116–8121, Sep. 1996.

[27] P. Baumgartner, C. Engel, G. Böhm, and G. Abstreiter, "Franz-Keldysh effect in lateral GaAs/AlGaAs based *npn* structures," *Appl. Phys. Lett.*, vol. 70, pp. 2876–2878, May 1997.

[28] J. M. Shah, Y.-L. Li, Th. Gessmann, and E. F. Schubert, "Experimental analysis and theoretical model for anomalously high ideality factors $(n >> 2.0)$ in AlGaN–GaN p-n junction diodes," *J. Appl. Phys.*, vol. 94, pp. 2627–2630, Aug. 2003.

[29] A. L. Beck, X. Guo, H.-D. Liu, A. Ghatak-roy, and J. C. Campbell, "Low dark count rate 4H-SiC Geiger mode avalanche photodiodes operated under gated quenching at 325 nm," *Proc. SPIE*, vol. 6372, p. 63720O, Oct. 2006.

Jose Luis Pau received the B.S. and M.S. degrees in physics from Universidad Autónoma de Madrid, Spain, in 1996 and 1998, respectively, and the Ph.D. degree from Universidad Politécnica de Madrid (UPM), Spain, in 2003.

From 2002 to 2006, he was a Research Assistant Professor in the Department of Electrical Engineering, UPM. He is currently a Fulbright Scholar at the Center for Quantum Devices, Northwestern University, Evanston, IL. His current research involves the development of UV single-photon detectors based on III-nitrides.

Ryan McClintock received the B.S. and Ph.D. degrees in electrical engineering from Northwestern University, Evanston, IL, in 2001 and 2007, respectively.

He is currently a Research Assistant Professor at the Center for Quantum Devices, Northwestern University. His research focuses on wide bandgap III-Nitrides for the development of ultraviolet photodetectors, lasers, and LEDs.

Can Bayram (M'00) received the B.S. degree in electrical engineering from Bilkent University, Ankara, Turkey, in 2005. He is currently pursuing the Ph.D. degree in the Electrical Engineering and Computer Science Department at the Center for Quantum Devices of Northwestern University, Evanston, IL.

His current research interests include the growth, fabrication, and characterization of (Al,Ga,In)N-based optoelectronic devices.

Kathryn Mayes received the B.S. degree in electrical engineering from Northwestern University, Evanston, IL in 2002, where she is currently working towards the Ph.D. degree in the Electrical Engineering and Computer Science Department.

She has been a member of Northwestern's Center for Quantum Devices since 2002 where her research interests are III-Nitride device processing and fabrication.

Donald Silversmith (F'03) received the Ph.D. degree in materials science from Massachusetts Institute of Technology (MIT), Cambridge, MA, in 1969.

Since then, he has held positions with Bell Laboratories, North American Philips, MIT Lincoln Laboratory, and the National Science Foundation, and has had short-term appointments with NASA and the Naval Research Laboratory. In 1988, he joined the Electrical and Computer Engineering faculty of Wayne State University, Detroit, MI, where he served for 15 years. In 2003, he was the first IEEE Diplomacy Fellow assigned to the US Department of State. Since 2005, he is Program Manager for Electronic and Photonic Materials at the Air Force Office of Scientific Research, Arlington, VA.

Manijeh Razeghi (F'05) received the Doctorat d'Etat es Sciences Physiques degree from the Université de Paris, France, in 1980.

After heading the Exploratory Materials Laboratory at Thomson-CSF (now Thales), France, she joined Northwestern University, Evanston, IL, as a Walter P. Murphy Professor and Director of the Center for Quantum Devices in 1992. She is one of the leading scientists in the field of semiconductor science and technology, pioneering in the development and implementation of major modern epitaxial techniques such as MOCVD, VPE, gas MBE, and MOMBE for the growth of entire compositional ranges of III-V compound semiconductors. Her current research interest is nanoscale optoelectronic quantum devices.

Dr. Razeghi is a Fellow of SPIE, Fellow and Life Member of the Society of Women Engineers (SWE), Fellow of The International Engineering Consortium (IEC), Fellow of the Optical Society of America (OSA) and a Member of the Electrochemical Society, ACS, MRS, APS, OSA, AAAS, and the French Academy of Sciences and Technology.